Journal of Power Sources 196 (2011) 2346–2350

Contents lists available at ScienceDirect

Journal of Power Sources

journal homepage: www.elsevier.com/locate/jpowsour

Performance of Mg–14Li–1Al–0.1Ce as anode for Mg-air battery

Yibin Ma[a], Ning Li[a,b,*], Deyu Li[a], Milin Zhang[b], Xiaomei Huang[b]

[a] School of Chemical Engineering and Technology, Harbin Institute of Technology, West Street No. 92, Harbin 150001, PR China
[b] Key Laboratory of Superlight Materials and Surface Technology, Ministry of Education, Harbin Engineering University, Harbin 150001, PR China

ARTICLE INFO

Article history:
Received 23 March 2010
Received in revised form 15 June 2010
Accepted 21 July 2010
Available online 8 October 2010

Keywords:
Magnesium-air battery
Magnesium–lithium alloy
Anodic efficiency
Self-corrosion

ABSTRACT

In this research, a new Mg-air battery based on Mg–14Li–1Al–0.1Ce was prepared and the battery performance was investigated by constant current discharge test. The corrosion behavior of Mg, AZ31 and Mg–Li–Al–Ce were studied by self-corrosion rate measurement and potentiodynamic polarization measurement. The characteristics of Mg–Li–Al–Ce after discharge were investigated by electrochemical impedance spectroscopy (EIS), scanning electron microscopy (SEM) and X-ray diffraction (XRD). The results show that Mg–Li–Al–Ce is more active than Mg and AZ31. The self-corrosion rate is found to be in the order: Mg–Li–Al–Ce < Mg < AZ31. It has been observed that the Mg-air battery based on Mg–Li–Al–Ce offers higher operating voltage, anodic efficiency and capacity than those with Mg and AZ31. SEM and EIS results show that the discharge product of Mg–Li–Al–Ce is loosely adhered to the alloy surface, and thus Mg–Li–Al–Ce could keep high discharge activity during discharge.

1. Introduction

Because of high theoretical voltage, high specific energy, low cost, light weight, and no pollution, Mg-air battery is a promising power source and energy storage device [1–3]. However, the Mg-air battery is currently still not as popular as Al-air battery and Zn-air battery. The major problem is that Mg anode exhibited some less attractive properties, such as severe self-corrosion and negative difference effect (NDE) during battery discharge. This wasteful self-corrosion and NDE resulted in severe capacity loss and low anodic efficiency, and these disadvantages have delayed the development of Mg-air battery and limited its commercial exploitation. One way to enhance the Mg anode performance is to alloy Mg with other elements.

In the alloying process, doping the Mg with other elements such as Al, Zn, Hg, and Ga are studied [4–6], and some Mg alloys (like AZ31, AZ61, Mg–Al–Zn–Zr) have been applied in Mg battery [7–12]. However, the idea of alloying Li with Mg is interesting, in theory, Mg–Li alloys have more negative standard electrode potential vs. standard hydrogen electrode, higher Faradic capacity and higher specific energy than other Mg alloys, and a few reports are available on the possibility of exploiting Mg–Li alloys as battery anode [13–16]. Furthermore, addition of Li above 10.5% could change the crystalline structure of Mg–Li alloys from hexagonal close-packed to cubic and increase their ductility [17]. Consequently, Mg–Li alloys could be considered as potential battery anode used in Mg-air battery, and it is of interest to study the discharge performance of Mg-air battery based on Mg–Li alloys.

Hence, in this study, the performance of Mg-air battery based on Mg–Li–Al–Ce was investigated. The electrochemical characteristic of Mg–Li–Al–Ce was studied by potentiodynamic polarization measurement and loss weight measurement. Electrochemical impedance spectroscopy, scanning electron microscopy and X-ray diffraction were used to examine the characteristics of Mg–Li–Al–Ce after discharge.

2. Experiment

2.1. Materials and self-corrosion measurements

Mg, AZ31 and Mg–14Li–1Al–0.1Ce were supplied by the Key Laboratory of Superlight Materials and Surface Technology, Harbin Engineering University, and these alloys were cut to 20 mm × 20 mm × 1.5 mm. The samples were mechanically polished with SiC abrasive paper, degreased with acetone and washed with distilled water. The self-corrosion rate was estimated by weight loss method after immersed in the neutral 3.5 wt.% NaCl solution for 16 h.

2.2. Electrochemical measurements

A classical three electrode cell was used, the working electrodes were Mg, AZ31 and Mg–Li–Al–Ce, the counter electrode was platinum electrode, and the reference electrode was saturated calomel electrode (SCE). Electrochemical measurements included potentiodynamic polarization measurement (1 mV s^{-1}, −1.8 to −1 V vs. SCE)

* Corresponding author. Tel.: +86 0451 86413721; fax: +86 0451 86418270.
E-mail address: lininghit@263.net (N. Li).

0378-7753/$ – see front matter © 2010 Elsevier B.V. All rights reserved.
doi:10.1016/j.jpowsour.2010.07.097

and electrochemical impedance spectroscopy (EIS) measurement (0.1–10^5 Hz, at open circuit potential).

2.3. Battery test

The Mg-air batteries consisted of anode, cathode and electrolyte, where anodes were Mg, AZ31 and Mg–Li–Al–Ce, cathode was air electrode with sliver catalyst, and electrolyte was neutral 3.5 wt.% NaCl solution. The discharge performance of Mg-air batteries was studied by means of constant current discharge test, constant current discharge test was determined at current densities of 0.5, 2.5, 5 and 10 mA cm^{-2} for a duration of 16 h. The weight of anode consumed was determined from the weights of the anodes before and after discharge. After discharge at 10 mA cm^{-2}, the discharge product of Mg–Li–Al–Ce deposited in electrolyte was filtered, and dried with vacuum condition.

2.4. SEM and XRD measurements

The surface morphologies of Mg–Li–Al–Ce after discharge were examined by scanning electron microscopy (SEM) (FEI Quanta 200F) with all samples being sputtered with gold. The phase composition of Mg–Li–Al–Ce alloy and its discharge product deposited in electrolyte were investigated by X-ray diffraction (XRD) using Cu Kα radiation.

3. Results and discussion

3.1. Phase composition of Mg–Li–Al–Ce alloy

Fig. 1 shows the XRD patterns of Mg–14Li–1Al–0.1Ce alloy, three strong diffraction peaks were observed, peaking at around $2\theta = 35.5–36.5^\circ$, $51.5–52.5^\circ$ and $64.5–65.5^\circ$, respectively. Compared with the standard diffraction peaks of Li_3Mg_7 (JCPDS card no. 65-6742), it could be seen that the main component of alloy was Li_3Mg_7, which is marked as β phase in Mg–Li phase diagram [18]. In addition, a little of $CeAl_2$ was found in Fig. 1.

3.2. Potentiodynamic polarization and self-corrosion rate

Fig. 2 presents the potentiodynamic polarization curves of Mg, AZ31 and Mg–Li–Al–Ce measured in 3.5 wt.% NaCl solution. The corrosion potential of Mg–Li–Al–Ce (−1.625 V) is more negative than that of Mg (−1.572 V) and AZ31 (−1.505 V), which means that Mg–Li–Al–Ce has higher electrochemical activity. The anodic current of Mg–Li–Al–Ce near the corrosion potential region is higher than that of Mg and AZ31, implying that Mg–Li–Al–Ce is less corrosion resistant than Mg and AZ31. Table 1 shows the self-corrosion rate of Mg, AZ31 and Mg–Li–Al–Ce, which is obtained by weight loss measurement in 3.5 wt.% NaCl solution. As illustrated in Table 1, Mg–Li–Al–Ce shows much lower self-corrosion rate than Mg and AZ31. Based on the above results, in contrast to Mg and AZ31, Mg–Li–Al–Ce could be used in Mg-air battery as anode, because of its low self-corrosion rate and high electrochemical activity, as well as good formability [19].

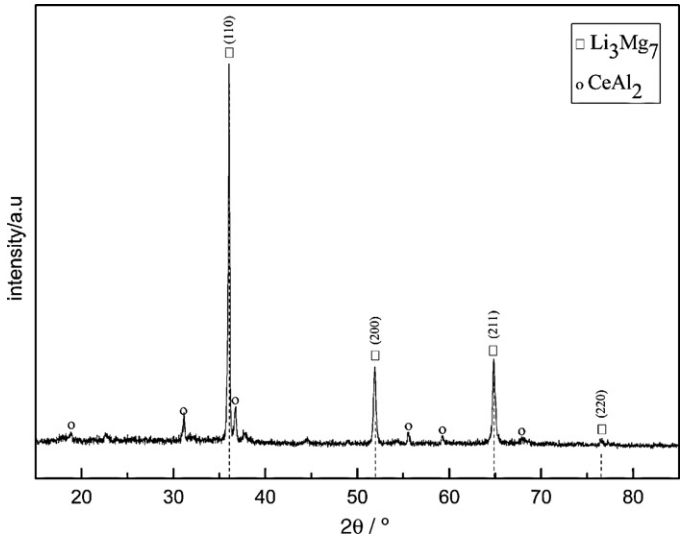

Fig. 1. XRD pattern of Mg–Li–Al–Ce alloy. The dash line is the standard diffraction peaks of Li_3Mg_7 based on JCPDS card no. 65-6742.

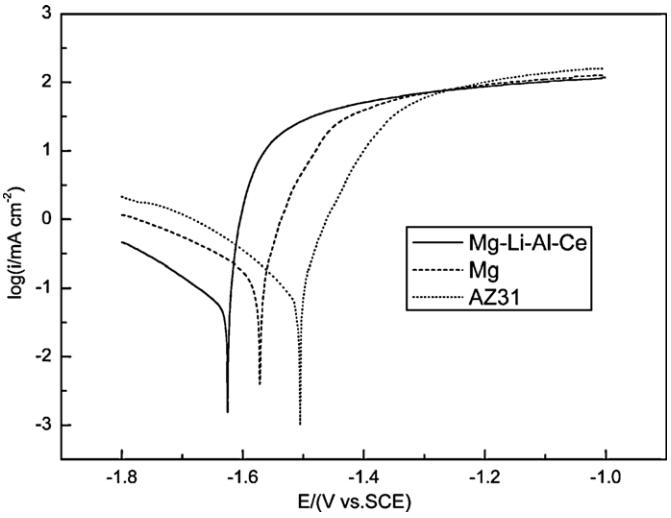

Fig. 2. Potentiodynamic polarization curves for Mg, AZ31 and Mg–Li–Al–Ce measured in 3.5% NaCl solution at a scan rate of 1 mV s^{-1}.

3.3. Magnesium-air battery performance

Fig. 3 shows the discharge behavior of Mg-air battery with different anodes at various constant current densities of 0.5, 2.5, 5 and 10 mA cm^{-2}. The voltage–time curves are similar for all the samples. The operating voltage decreased rapidly in the early discharging stage, which is caused by a discharge product film formed on the anode surface, and then reached to an approximate constant value. It should be noted that the operating voltage of Mg-air battery with Mg–Li–Al–Ce was higher than those of Mg and AZ31 at various discharge current densities. Moreover, as shown in Fig. 3(d), the operating voltage of Mg-air battery with AZ31 decreases rapidly to 0 V after 800 min of discharge, which means that the AZ31 anode was completely consumed.

Table 2 summarizes the performance of the above batteries at various current densities of 0.5, 2.5, 5 and 10 mA cm^{-2}. As shown in Table 2, the Mg-air battery with Mg–Li–Al–Ce displays higher anodic efficiency and higher specific discharge capacity than those of Mg and AZ31. The anodic efficiency of Mg–Li–Al–Ce is 15–40% higher than that of Mg and 20–50% higher than that of

Table 1
Corrosion rates of different materials in neutral 3.5 wt.% NaCl solution.

Material	Corrosion rate (mg cm^{-2} h^{-1})
Mg–Li–Al–Ce	0.35
Mg	0.53
AZ31	1.44

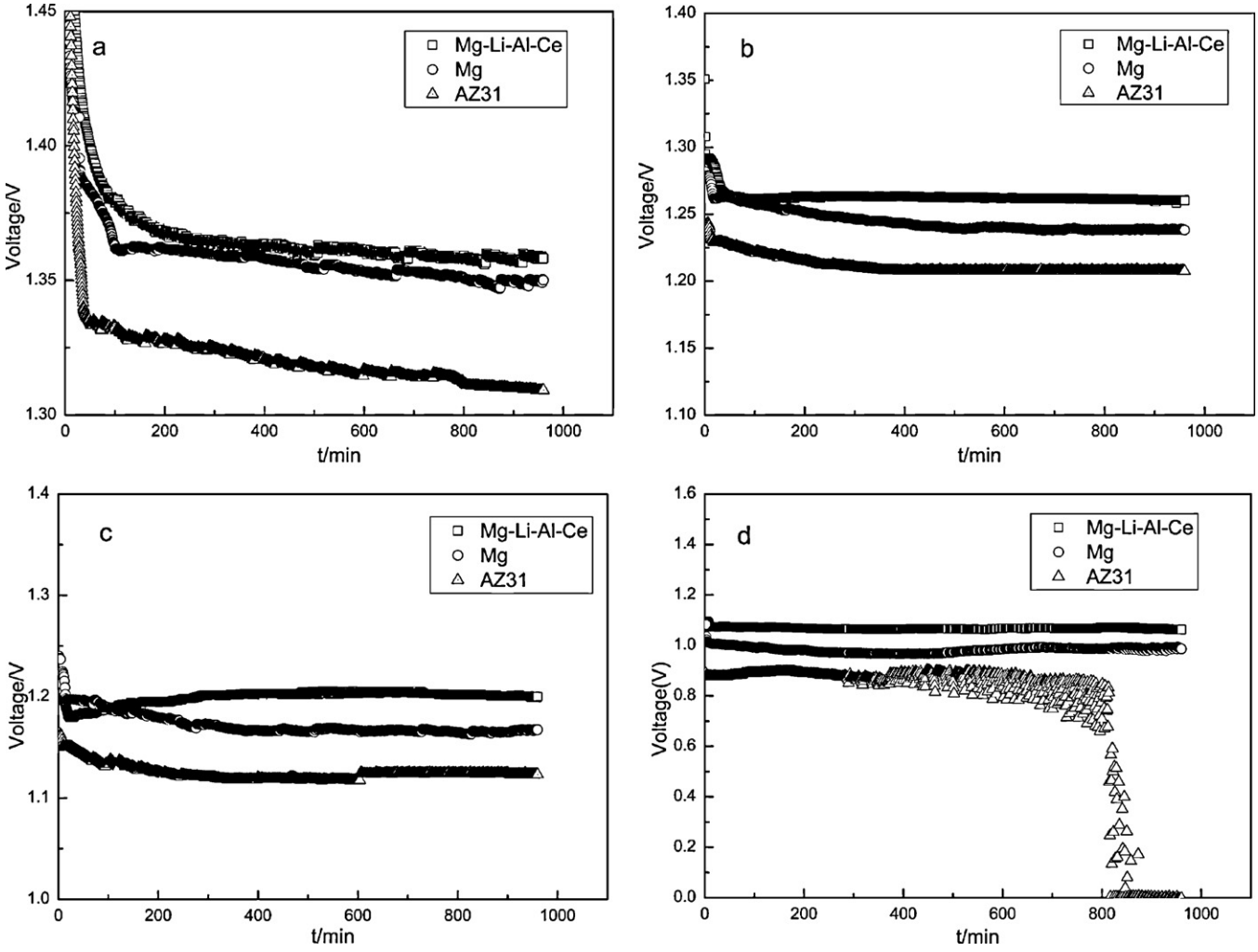

Fig. 3. Discharge behavior of Mg-air battery with different anodes at different current. (a) 0.5 mA cm^{-2}, (b) 2.5 mA cm^{-2}, (c) 5 mA cm^{-2}, and (d) 10 mA cm^{-2}.

AZ31, the increase in anodic efficiency leads to the increase in specific discharge capacity. Among all the samples, at a current density of 2.5 mA cm^{-2}, the best performance of Mg-air battery with Mg–Li–Al–Ce is obtained, the working voltage is 1.261 V, anodic efficiency is 85.2% and specific discharge capacity is 2072 mAh g^{-1}. Improved discharge characteristics may be due to the cubic crystal structure of this alloy, which results in an increase of hydrogen evolution overpotential and a decrease of self-corrosion [13–15].

3.4. Surface analysis after discharge

The surface morphologies and the cross section morphologies of Mg–Li–Al–Ce after discharge at various current densities for 6 h in 3.5 wt.% NaCl solution were obtained by scanning electron microscopy examination. The results are shown in Fig. 4, it could be seen that the discharge products film formed on the Mg–Li–Al–Ce surface was loose with many pores and cracks. The loosely discharged products allowed the electrolyte to penetrate through, as a

Table 2
The discharge performance of Mg-air battery with different anode.

Current density (mA cm^{-2})	Material	Operating voltage (V)	Anodic efficiency (%)	Specific discharge (mAh g^{-1})
0.5	Mg–Li–Al–Ce	1.371	61.6	1500
	Mg	1.361	34.4	759
	AZ31	1.332	17.3	394
2.5	Mg–Li–Al–Ce	1.272	85.2	2072
	Mg	1.239	43.7	964
	AZ31	1.207	32.2	733
5	Mg–Li–Al–Ce	1.201	73.5	1788
	Mg	1.166	58.4	1288
	AZ31	1.125	49.4	1125
10	Mg–Li–Al–Ce	1.065	66.8	1626
	Mg	0.983	54.9	1210
	AZ31	0.836	44	1002

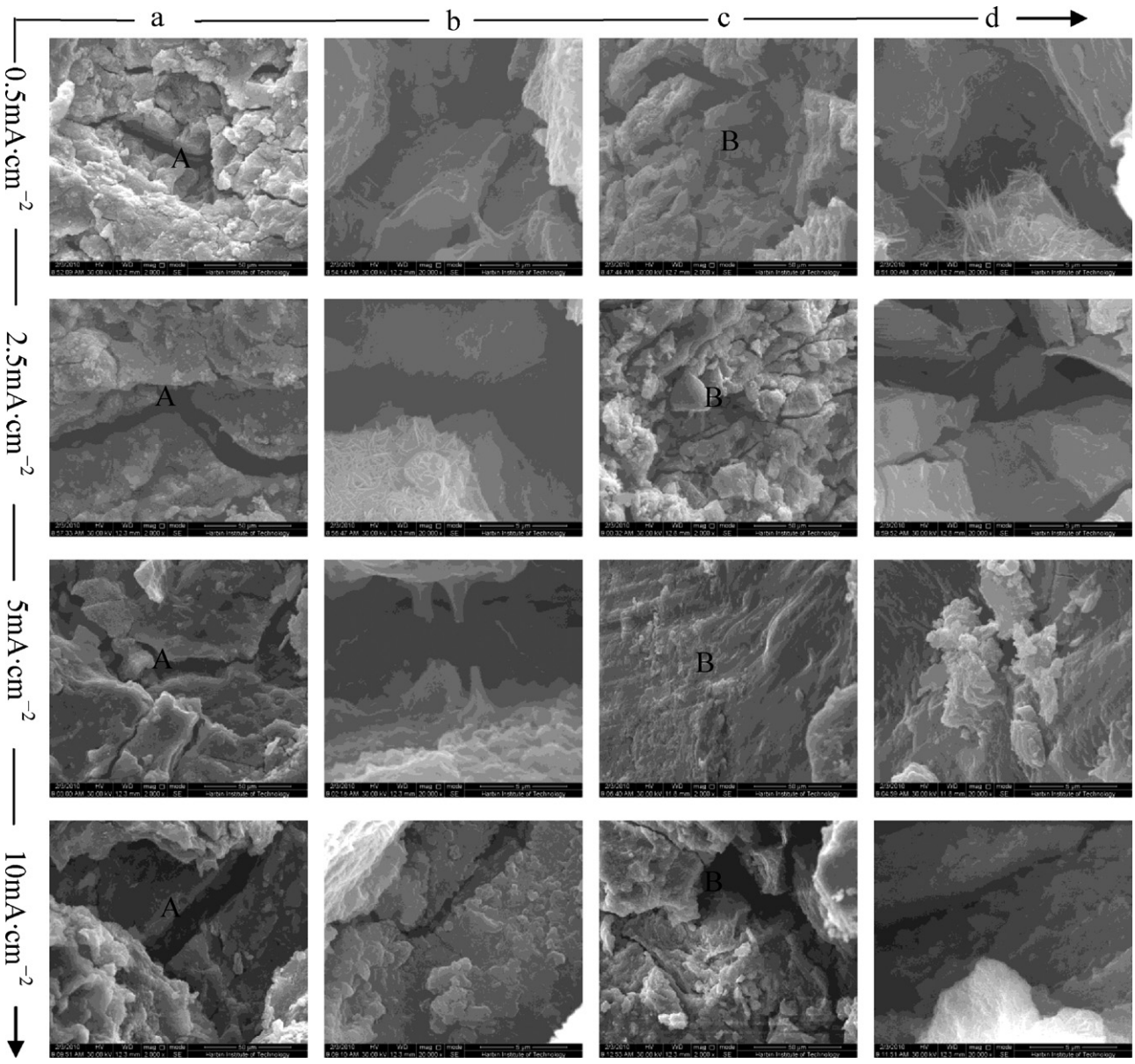

Fig. 4. SEM micrographs of Mg–Li–Al–Ce obtained after discharge at various current densities for 6 h in 3.5 wt.% NaCl solution. (a) The surface of samples, (b) zoom of A zone, (c) the cross section of samples, and (d) zoom of B zone.

result, Mg–Li–Al–Ce retains large reaction surface during discharge, which enabled Mg–Li–Al–Ce to keep high discharge activity. On the other hand, the discharge products of Mg–Li–Al–Ce at various current densities existed in different forms on the alloy surface.

The X-ray diffraction (XRD) was used to examine the composition of discharge product of Mg–Li–Al–Ce deposited in electrolyte after discharged at 10 mA cm^{-2}. The XRD analysis is shown in Fig. 5. Several diffraction peaks were observed, peaking at around 2θ = 18–19°, 32.5–33.5°, 37.5–38.5°, 50.5–51.5°, 58.5–59.5°, 61.5–62.5°, 68–69°, 71.5–72.5° and 80–82°, respectively. Compared with the standard diffraction peaks of $Mg(OH)_2$ (JCPDS card no. 44-1482), it was indicated that the discharge product was $Mg(OH)_2$. It should be noted that there is no reaction product of Li; the possible reason is that the discharge product of Li can dissolve in electrolyte.

3.5. Electrochemical impedance spectroscopy

The electrochemical impedance spectroscopy measurements (EIS) were performed after Mg–Li–Al–Ce was discharged at various current densities for 6 h. The EIS plots are shown in Fig. 6. The EIS plots consisted of two loops. The high frequency loop might be resulted from charge transfer, the middle frequency loop might be attributed to mass transport relaxation in the solid phase (an aggregating layer) on the alloy surface [20–23]. The EIS plots for the samples discharged at different current densities can be equivalent to the circuit as shown in Fig. 7. The constant phase elements Q_1 and Q_2 were used to compensate for the non-homogeneity in the system [24]. R_s was the solution resistance, R_t was the charge transfer resistance, Q_1 represented the electric double layer capac-

Table 3
EIS fitting results of Mg–14Li–1Al–0.1Ce alloy after discharged at various current densities for 6 h in 3.5 wt.% NaCl solution.

Current density (mA cm^{-2})	R_s (Ω cm^{-2})	R_t (Ω cm^{-2})	R_f(Ω cm^{-2})
0.5	2.617	35.92	10.88
2.5	1.889	31.77	25.45
5	1.686	22.51	45.32
10	3.347	29.59	15.16

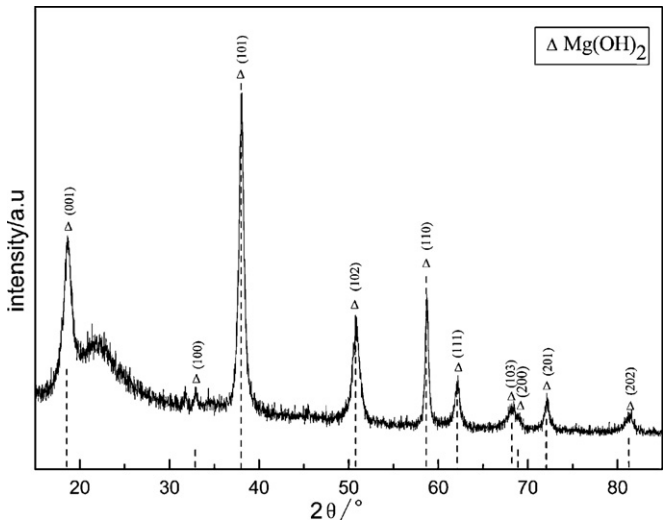

Fig. 5. XRD pattern of discharge product of Mg–Li–Al–Ce. The dash line is the standard diffraction peaks of $Mg(OH)_2$ based on JCPDS card no. 44-1482.

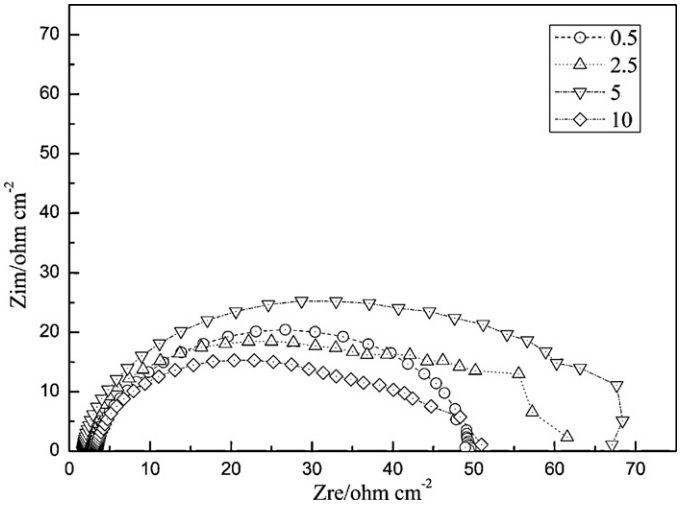

Fig. 6. EIS patterns of Mg–14Li–1Al–0.1Ce alloy after discharge at various current densities for 6 h in 3.5 wt.% NaCl solution.

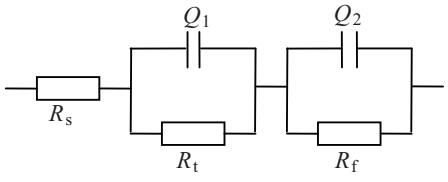

Fig. 7. Equivalent circuits of EIS plots.

ity, R_f represented the film resistance and Q_2 represented the film capacity. As for coatings, this resistance could be attributed to the electrolytic resistance in the pores of the layer (conductive pathways). The EIS fitting results are listed in Table 3. As shown in Table 3, the variation of R_f indicated that the discharge product layer formed on the Mg–Li–Al–Ce alloy surface was different at various discharge current densities. The low R_t values represent that the discharge product layer could not afford strong protection, consequently Mg–Li–Al–Ce could keep high discharge activity during discharge. The results above are in good consistent with the results of SEM.

4. Conclusions

We investigated the corrosion behavior and discharge performance of Mg, AZ31 and Mg–Li–Al–Ce in 3.5 wt.% NaCl solution. Compared with Mg and AZ31, Mg–Li–Al–Ce has higher electrochemical activity and lower self-corrosion rate. Using Mg–Li–Al–Ce as anode could improve the performance of Mg-air battery, and solve the problem of severe capacity loss and low anode utilization efficiency. At a current density of 2.5 mA cm^{-2}, the operate voltage of Mg-air battery with Mg–Li–Al–Ce anode is 1.272 V, the specific discharge capacity is 2076 mAh g^{-1}, and the anodic utilization efficiency is 85.2%. The discharge products of Mg–Li–Al–Ce remained on the alloys surface were loose, which is partially responsible for the high discharge activity of Mg–Li–Al–Ce during discharge. The discharge product of Mg–Li–Al–Ce deposited in electrolyte is $Mg(OH)_2$.

Acknowledgements

This work was financially supported by Key Laboratory of Superlight Material and Surface Technology of Ministry of Education and Harbin Engineering University.

References

[1] K.F. Blurton, A.F. Sammells, J. Power Sources 4 (1979) 263–279.
[2] D. Linden, T.B. Reddy, Handbook of Batteries, 3rd ed., McGraw-Hill, 2002.
[3] W.Y. Li, C.S. Li, C.Y. Zhou, H. Ma, J. Chen. Angew. Chem. Int. Ed. 45 (2006) 6009–6012.
[4] O. Yamamoto, T. Kanbara, Magnesium Alloy Battery, 2001 (US6265109B1).
[5] Y. Feng, R.C. Wang, K. Yu, C.Q. Peng, J.P. Zhang, C. Zhang, J. Alloys Compd. 473 (2009) 215–219.
[6] R. Udhayan, D.P. Bhatt, J. Power Sources 53 (1996) 103–107.
[7] S. Tamulevičius, R. Dargis, J. Power Sources 72 (1998) 9–13.
[8] M.G. Medeiros, E.G. Dow, J. Power Sources 80 (1999) 78–82.
[9] M.G. Medeiros, R.R. Bessette, C.M. Deschenes, C.J. Patrissi, L.G. Carreiro, S.P. Tucker, D.W. Atwater, J. Power Sources 136 (2004) 226–231.
[10] R. Renuka, J. Power Sources 87 (2000) 4–11.
[11] R. Thirunakaran, S. Vasudevan, A. Sivashanmugam, S. Gopukumar, J. Power Sources 148 (2005) 112–115.
[12] R. Balasubramanian, A. Veluchamy, N. Venkatakrishnan, R. Gangadharan, J. Power Sources 56 (1995) 197–199.
[13] M. Sahoo, J.T.N. Atkinson, J. Mater. Sci. 17 (1982) 3564–3574.
[14] A. Sivashanmugam, T. Sremkumar, N.G. Renganathan, S. Gopukumar, J. Appl. Electrochem. 34 (2004) 1135–1139.
[15] D.X. Cao, L. Wu, G.L. Wang, Y.Z. Lv, J. Power Sources 177 (2008) 624–630.
[16] D.X. Cao, L. Wu, G.L. Wang, Y.Z. Lv, J. Power Sources 183 (2008) 799–804.
[17] O. Sivakesavam, Y.V.R.K. Prasad, Mater. Sci. Eng. A 323 (2002) 270–277.
[18] G.S. Song, M.V. Kral, Mater. Charact. 54 (2005) 279–286.
[19] M.V. Kral, B.C. Muddleb, J.F. Nie, Mater. Sci. Eng. A 460–461 (2007) 227–232.
[20] L.L. Gao, C.H. Zhang, M.L. Zhang, X.M. Huang, N. Sheng, J. Alloys Compd. 468 (2009) 285–289.
[21] M. Anik, G. Celikten, Corros. Sci. 49 (2007) 1878–1894.
[22] G. Galicia, N. Pébère, B. Tribollet, V. Vivier, Corros. Sci. 51 (2009) 1789–1794.
[23] X.W. Guo, J.W. Changa, S.M. He, W.J. Ding, X.S. Wang, Electrochim. Acta 52 (2007) 2570–2579.
[24] Y.W. Song, D.Y. Shan, R.S. Chen, E.H. Han, Corros. Sci. 51 (2009) 1087–1094.